

A reflection origin for the soft and hard X-ray excess of Ark 120

E. Nardini,^{1,2,3*} A.C. Fabian,³ R.C. Reis³ and D.J. Walton³

¹ *Dipartimento di Fisica e Astronomia - Sezione di Astronomia, Università di Firenze, L.go E. Fermi 2, 50125 Firenze, Italy*

² *INAF - Osservatorio Astrofisico di Arcetri, L.go E. Fermi 5, 50125 Firenze, Italy*

³ *Institute of Astronomy, Madingley Road, Cambridge CB3 0HA*

Released XXXX XXXX XX

ABSTRACT

Over the last few years several models have been proposed to interpret the widespread soft excess observed in the X-ray spectra of type 1 active galactic nuclei (AGN). In particular, reflection from the photoionized accretion disc blurred by relativistic effects has proven to be successful in reproducing both the spectral shape and the variability pattern of many sources. As a further test to this scenario we present the analysis of a recent ~ 100 ks long *Suzaku* observation of Arakelian 120, a prototypical ‘bare’ Seyfert 1 galaxy in which no complex absorption system is expected to mimic a soft excess or mask the intrinsic properties of this key component. We show that a reflection model allowing for both warm/blurred and cold/distant reprocessing provides a self-consistent and convincing interpretation of the broadband X-ray emission of Ark 120, also characterized by a structured iron feature and a high-energy hump. Although warm absorbers, winds/outflows and multiple Comptonizing regions may play significant roles in sources with more spectral complexity, this case study adds evidence to the presence of blurred disc reflection as a basic component of the X-ray spectra of type 1 AGN.

Key words: galaxies: active – galaxies: individual: Ark 120 – X-rays: galaxies.

1 INTRODUCTION

Over the 2–10 keV energy range, the X-ray spectra of type 1 active galactic nuclei (AGN) are usually well-reproduced by a power-law component, which is believed to originate from the Comptonization of cold seed photons in a hot coronal region above the accretion disc, according to the so-called two-phase model (Haardt & Maraschi 1991, 1993). When extrapolated to the lower energies, the simple power-law trend fails to account for the extra emission systematically observed in unabsorbed Seyfert galaxies (after Arnaud et al. 1985). Due to its extremely smooth shape, this soft excess turns out to be consistent with several physical models. In analogy with the high/soft states of galactic black hole binaries (Remillard & McClintock 2006), dominated by thermal emission from the disc, the initial attempts at modelling the AGN soft excess were based on single or multicolour blackbody components. Although well-fitting, this thermal continuum requires a temperature far higher than that expected for a standard thin disc around a supermassive black hole. Moreover, when tested on large AGN samples, the characteristic temperature is found to be remarkably constant over almost

four orders of magnitude in the black hole mass, in spite of very different Eddington rates (e.g. Crummy et al. 2006, and references therein; Miniutti et al. 2009). A thermal soft excess does not even comply with the Stefan–Boltzmann law for the largest variations in the overall luminosity (Ponti et al. 2006), and the inferred size of the emitting region is usually unreasonably small with respect to the gravitational radius ($r_g = GM/c^2$).

In terms of spectral decomposition, similar results can be obtained by invoking the Comptonization of disc photons in a cold and optically thick plasma (Page et al. 2004). This raises questions on the nature of the X-ray corona. In the case of two detached Comptonizing regions with different physical properties (e.g. Dewangan et al. 2007), most of the limitations of the thermal scenario described above also apply to the ‘soft’ corona. On the other hand, a single plasma with hybrid thermal/non-thermal electron distribution (Coppi 1999) may give rise to both the soft excess and the hard power-law component.

Alternatively, the universal shape of the soft X-ray emission has been linked to atomic physics: Gierliński & Done (2004) suggested that the soft excess is actually a fake continuum component due to a broad absorption trough at ~ 2 –5 keV, arising in partially ionized gas along the line of sight subject

* E-mail: emanuele@ast.cam.ac.uk

to high velocity smearing. The latest simulations, however, prove that the properties of any realistic accretion disc wind are not able to reproduce the observed smoothness of the soft excess (Schurch & Done 2007; Schurch, Done & Proga 2009). Another viable explanation is that of reflection from the photoionized surface layers of the accretion disc itself, where the relativistic motion of the infalling matter provides the blurring of the narrow atomic features (Fabian et al. 2002; Crummy et al. 2006). This model occasionally implies a strong suppression of the intrinsic power law in order to account for a prominent soft excess, as justified in the context of strong gravitational light bending (Miniutti & Fabian 2004).

On sheer statistical grounds all the interpretations outlined so far yield acceptable results (Sobolewska & Done 2007). To pursue further this kind of study, access is needed to energies beyond ~ 10 keV, where the physical models make different predictions. The advent of *Suzaku* (Mitsuda et al. 2007) and its hard X-ray detector (HXD; Takahashi et al. 2007) has made it possible to put solid spectral constraints up to ~ 70 keV, opening a new era of AGN observations. Concerning the soft excess, it should also be noticed that the possible presence of complex and variable absorption can mask the intrinsic appearance of this critical component. Indeed, warm absorbers are very common among type 1 AGN (Crenshaw, Kraemer & George 2003; Blustin et al. 2005). It is therefore desirable to select a target with the cleanest view of the nuclear regions.

Arakelian 120 ($z = 0.0327$) is a rare case of a ‘bare’ Seyfert galaxy, hence it represents the optimal candidate to test whether the soft excess is a signature of blurred reflection from the inner accretion disc. No evidence for reddening is found in the infrared (Ward et al. 1987), and ultraviolet observations establish that Ark 120 is devoid of intrinsic absorption (Crenshaw et al. 1999). In the soft X-ray band the source has been shown to have a steep spectrum by both *EXOSAT* (Turner & Pounds 1989) and *ROSAT* (Brandt et al. 1993), while the *XMM-Newton* Reflection Grating Spectrometer data allow stringent upper limits (~ 1 – 2 orders of magnitude lower than those of usual Seyfert 1s) to be placed on the ionic column densities of any possible warm absorber (Vaughan et al. 2004). It is worth emphasizing that Ark 120 is a broad-line Seyfert 1 (BLS1) galaxy, whereas the soft excess has been long associated with narrow-line sources only. NLS1s are rather eccentric objects, known for their very steep X-ray spectrum (Boller, Brandt & Fink 1996), high accretion rate (Grupe 2004, and references therein), large-amplitude X-ray variability on short timescales (Gallo et al. 2004), metal overabundance (Shemmer & Netzer 2002; Fabian et al. 2009) and enhanced star formation (Sani et al. 2010). Ark 120 is an outstanding counter example of a normal BLS1 with a prominent soft excess, ensuring as such a completely unbiased exploration of this component.

This work is organized as follows: Section 2 concerns the observation and data reduction; our results are presented and fully discussed in Section 3, while in Section 4 we summarize our conclusion and outline the future research.

2 OBSERVATION AND DATA REDUCTION

Ark 120 was observed by *Suzaku* on 2007 April 1–3 in the HXD nominal position, with a resulting net exposure of ~ 101 ks for the X-ray imaging spectrometer (XIS; Koyama et al. 2007) and ~ 89 ks for the HXD/PIN detector. Events were collected by the three operational XIS CCDs in both 3×3 and 5×5 editing modes (71 and 30 ks exposures, respectively). Following the standard procedure illustrated in the *Suzaku* Data Reduction Guide,¹ we used the HEASOFT FTTOOLS 6.8 package to obtain a new set of clean event files for each detector, editing mode and telemetry by reprocessing the unfiltered events with the latest calibrations. The source spectra and light curves were extracted from circular regions with radius of ~ 3.5 arcmin (200 pixels) centred on the target, while the background was evaluated on the same chip from adjacent regions devoid of significant contamination. Finally, the source and background spectra from the two front-illuminated detectors (XIS0 and XIS3), as well as the response files generated through the ‘xisresp’ script, were merged and rebinned by a factor of 4.

Concerning the HXD/PIN data reduction, we again reprocessed the unfiltered event files using the standard tools and got the output spectrum by running the ‘hxdpinxbpi’ script, which takes into account the contribution of both the non X-ray and the cosmic X-ray background and applies the dead time correction. This returned a source count rate of $(12.1 \pm 0.3) \times 10^{-2} \text{ s}^{-1}$, corresponding to 18.7 per cent of the PIN total counts.

The spectral analysis has been performed using the XSPEC v12.6 fitting package, and involves only the 0.5–12 keV energy range of the two front-illuminated XIS detectors; indeed, the 1.7–2.0 keV interval appears to be strongly affected by systematic calibration uncertainties around the instrumental silicon K-edge, hence it has been excluded. The XIS1 back-illuminated spectrum has been employed throughout as an independent check. The source is confidently detected at high energy up to ~ 40 – 50 keV; we have therefore considered the conservative 12–40 keV range of the HXD/PIN spectrum. In order to allow the use of χ^2 minimization during the spectral fitting, the XIS data were grouped so that each energy channel contains no less than 20 counts, while a minimum of 50 counts per bin was adopted for the HXD/PIN spectrum. The uncertainties reported in this work correspond to the 90 per cent confidence intervals ($\Delta\chi^2 = 2.71$) for the single parameter of interest. Fluxes and count rates are given at the 1σ level.

3 DATA ANALYSIS AND DISCUSSION

In Fig. 1 we show the data/model ratio plot obtained by fitting the *Suzaku* spectrum of Ark 120 with a simple power law over the 2.5–5.5 keV range. The output is obviously model-dependent, especially with respect to the magnitude of the soft and hard excess; none the less, both the sizable spectral curvature and the prominent iron emission are clearly brought out. Our analysis is first aimed at a detailed inspection of the latter feature, and is subsequently extended to the whole 0.5–40 keV energy range. Also, we briefly examine

¹ <http://heasarc.gsfc.nasa.gov/docs/suzaku/analysis/abc/>

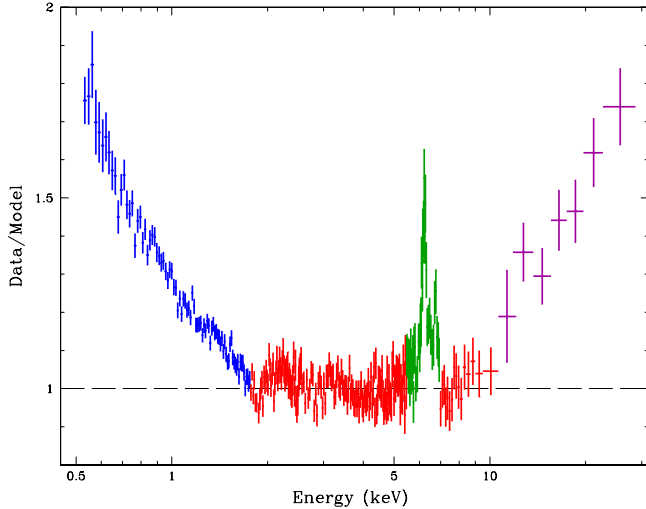


Figure 1. The *Suzaku* XIS0+XIS3 and PIN spectra of Ark 120 plotted as a data/model ratio after fitting the 2.5–5.5 keV range only with a power law. This sketch, though model-dependent, is straightforward in bringing out both the prominent iron feature at ~ 6 keV and the overall spectral curvature, the latter suggesting the presence of a smooth soft excess below 2 keV and of a broad reflection hump beyond 10 keV. (The spectral data shown throughout this work have been rebinned for plotting purposes only).

the source variability, and review the previous *XMM-Newton* observation of Ark 120 in the light of the new evidence from the present work.

3.1 Iron K-shell emission

After excluding the 5–7.5 keV region characterized by the complex iron feature, the 2.5–12 keV spectrum has been fitted with a basic model consisting of a power law modified by Galactic absorption only. Despite the apparent lack of local obscuration in Ark 120, the foreground column density towards the source is quite large due to its low Galactic latitude ($b = -21^\circ 13'$). Two different values for N_{H} have been determined from the $\lambda 21$ -cm neutral hydrogen emission maps, i.e. $0.98 \times 10^{-21} \text{ cm}^{-2}$ (Kalberla et al. 2005) and $1.26 \times 10^{-21} \text{ cm}^{-2}$ (Dickey & Lockman 1990). Throughout this work, Galactic absorption has been modelled by means of the TBABS code (Wilms, Allen & McCray, 2000), assuming the estimates above to be the extremes of the allowed range for N_{H} . We will briefly return to this point later on, since for now the selection of a precise value of N_{H} does not affect the study of iron emission around 6 keV.

The shape of this feature is shown in the top panel of Fig. 2. Different attempts have been made in order to disentangle the components of such a structured profile. Here we consider the following four cases: two narrow lines; three narrow lines; two narrow lines and a disc line; two broad lines.

1) A model including only a couple of narrow gaussian lines of width $\sigma = 10$ eV yields a statistically good fit to the data, with $\chi^2_{\nu}/\text{d.o.f.} = 0.869/283$. The lines are centred at ~ 6.42 and 6.96 keV in the source frame, and are consistent with the energy expected for K-shell emission from neutral and H-like iron; their equivalent widths (EW) are ~ 90 and 40 eV, respectively. However, this solution is clearly insuffi-

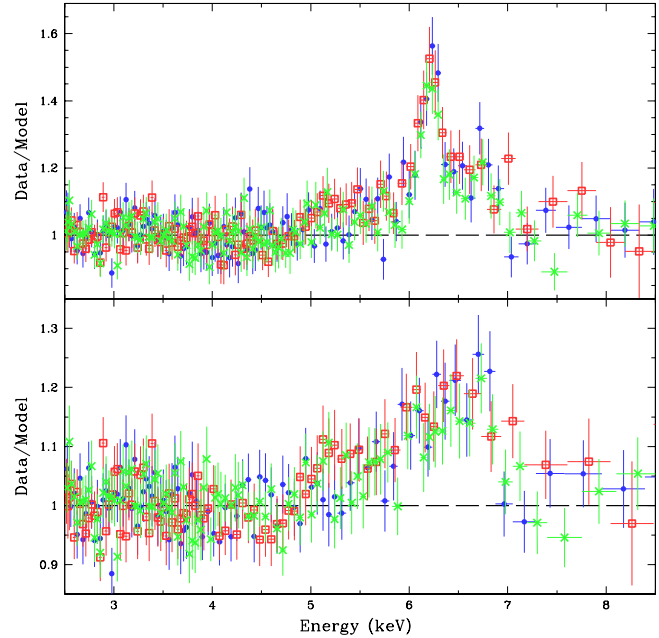


Figure 2. Top panel: the structured profile of iron K-shell emission obtained as a data/model ratio after fitting the 2.5–5.5 plus 7–12 keV energy range with a single power law. It is evident that two narrow gaussian components are not sufficient to reproduce the whole feature. The data from XIS0 (blue dots), XIS1 (red squares) and XIS3 (green crosses) are shown separately. Bottom panel: same as above, after removing the disc line component from the best fitting-model.

cient to reproduce the observed feature.

2) By adding another narrow line, the fit undergoes a considerable improvement ($\chi^2_{\nu}/\text{d.o.f.} = 0.789/281$). The new line has an energy of ~ 6.67 keV, driving a straightforward identification as He-like iron emission, and an EW of ~ 30 eV. But also this interpretation is not fully adequate.

3) In fact, the most successful way to fit the residuals left by the two narrow lines is to allow for a disc line, whose broadening is due to relativistic effects. By including in the model a LAOR profile (Laor 1991) we get an excellent fit of the whole iron emission feature ($\chi^2_{\nu}/\text{d.o.f.} = 0.686/280$). The shape of this skewed component is shown in the bottom panel of Fig. 2, and clearly exhibits the red elongated wing typical of lines arising from the inner disc, even if not as prominent as in the well-known case of MCG–6–30–15 (Miniutti et al. 2007). For this reason, it is not possible to constrain simultaneously all the line parameters (see Table 1): these include the disc inner radius (r_{in}) and inclination with respect to the line of sight and the emissivity index q (under the assumption of a radial emissivity profile $\epsilon(r) \propto r^{-q}$). None the less, we note that the best-fitting inner radius of $\sim 13 r_{\text{g}}$ does not necessarily require the extreme gravity regime typical of rapidly rotating black holes. It is important to stress that alternative explanations invoking a spectral upturn due to complex absorption effects, such as those proposed for the same MCG–6–30–15, are definitely not viable in the case of Ark 120.

4) In the latter stage, the properties of the two narrow lines are exactly the same as found in the original model. Thus, it is worth investigating another possibility by re-

Table 1. Best-fitting parameters for different models of the iron K-shell feature: 1) two narrow lines; 2) three narrow lines; 3) two narrow lines plus a LAOR disc line; 4) two broad lines. The asterisk-marked parameters have not been allowed to vary.

E_1^a	$6.42^{+0.02}_{-0.01}$	EW_1^b	89 ± 20
E_2^a	6.96 ± 0.03	EW_2^b	41 ± 12
σ^b	10^*	χ^2_ν	246/283
E_1^a	$6.42^{+0.01}_{-0.02}$	EW_1^b	86 ± 20
E_2^a	$6.67^{+0.04}_{-0.05}$	EW_2^b	26 ± 17
E_3^a	6.97 ± 0.03	EW_3^b	41 ± 22
σ^b	10^*	χ^2_ν	222/281
E_1^a	$6.42^{+0.01}_{-0.02}$	EW_L^b	123^{+77}_{-65}
E_2^a	$6.98^{+0.04}_{-0.03}$	q^c	3.0^*
σ^b	10^*	r_{in}^d	13^{+19}_{-7}
EW_1^b	61^{+25}_{-23}	r_{out}^d	400^*
EW_2^b	43^{+25}_{-24}	θ^e	40^*
E_L^a	$6.46^{+0.06}_{-0.07}$	χ^2_ν	192/280
E_1^a	6.42 ± 0.02	EW_1^b	137 ± 33
E_2^a	$6.94^{+0.04}_{-0.05}$	EW_2^b	64 ± 26
σ^b	113 ± 21	χ^2_ν	207/282

^a Line peak energy, in keV.^b Line (equivalent) width, in eV.^c Disc emissivity index, $\epsilon(r) \propto r^{-q}$.^d Disc inner/outer radius, in r_g units.^e Disc inclination, in degrees.

taining the basic template and allowing the width of the two lines to vary. The consequent fit refinement is not as significant as when a disc line is involved, being now $\chi^2_{\nu}/\text{d.o.f.} = 0.735/282$: the difference of $\Delta\chi^2 \simeq -15.2$ obtained with the loss of two degrees of freedom is not likely to be simply a chance improvement and supports the relativistic line detection. Moreover, although the double-peaked energy of the blended feature is still consistent within the errors with neutral and H-like iron emission (Table 1), the resulting width of $\sigma = 113(\pm 21)$ eV poses the question about the physical location wherein these lines arise. Such a value, in fact, corresponds to a full width at half-maximum (FWHM) broadening of $\sim 12 \times 10^3 \text{ km s}^{-1}$, which is a factor of ~ 2 larger than that observed in the optical permitted lines (FWHM H $\beta \simeq 5800 \text{ km s}^{-1}$; Wandel, Peterson & Malkan 1999). This could hint at a sort of X-ray broad-line region (BLR) internal to the optical one.

Any further discussion on the possible origin of these lines (either broad or narrow) is deferred to the next section, in which we address this issue within the context of X-ray reflection models. We are confident that relativistic effects are in place and have to be taken into account also when considering the entire spectral range, since all the interpretations of the iron emission profile in Ark 120 making no resort to a disc line turn out to be less successful and convincing.

3.2 Blurred reflection model

We now extend our analysis to the whole 0.5–40 keV energy range, in order to understand the origin of the spectral curvature.² Excess emission beyond ~ 20 –30 keV is usually

interpreted as due to the reprocessing of the primary X-ray radiation: the combination of photoelectric absorption and Compton scattering in the illuminated material gives rise to a broad reflection hump (e.g. George & Fabian 1991, and references therein). Besides this additional continuum component and iron fluorescence, below ~ 2 keV the reflected spectrum is expected to be dominated by a wealth of emission lines from oxygen and other abundant elements, like C, N, Ne, Mg, Si, S (Ross & Fabian 1993). Since it is fairly conceivable that in many cases the accretion flow itself acts as the most efficient *mirror*, depending on the ionization stage of the disc outer layers and on the relativistic motions of the inner regions, the stack of individual features can be blurred into the smooth shape of the soft excess.

As stated above, the slight spectral curvature observed at ~ 6 keV in Ark 120 cannot be explained as the product of (multiple) covering effects, suggesting instead the presence of a broad skewed profile within the iron emission feature and indicating a strong gravity regime. It is therefore reasonable to include in our general model two reflection components, for which we have used the self-consistent RELIONX table models of Ross & Fabian (2005): the first one is expected to arise from almost neutral material at great distance from the X-ray emitting region, likely situated on the dusty torus scale. The second one can be ascribed to the partially ionized surface of the disc, and has been convolved with the KDBLUR kernel in XSPEC to account for relativistic effects. The model obviously comprises the primary power law, absorbed by the Galactic column density, and also the two unresolved gaussian lines identified above, corresponding to neutral and H-like iron emission. Galactic absorption is found to be consistent with $N_H = 0.98 \times 10^{-21} \text{ cm}^{-2}$, and has been frozen accordingly.

The reflection templates include among their free param-

² The cross calibration between the XIS and PIN spectra has been fixed to the recommended value of 1.17.

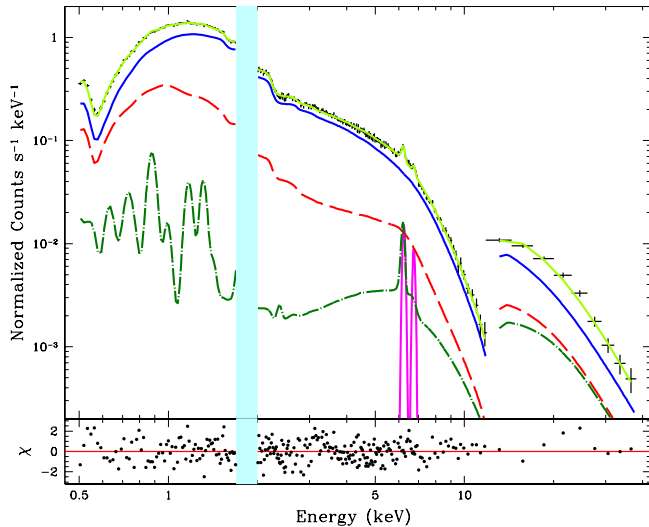


Figure 3. Top panel: *Suzaku* XIS and HXD/PIN spectrum of Ark 120 and best-fitting reflection model (light green solid line). The contribution of all the different components is disentangled: primary power law (blue), blurred (red, dashed) and distant (deep green, dot-dashed) reflection, narrow iron lines (magenta). The shaded 1.7–2 keV region has been excluded from the fit. Bottom panel: residuals in units of σ (the error bars have size one).

ters iron abundance (which has been assumed to be single-valued across the source), ionization state (described by the quantity $\xi = 4\pi F/n_H$, where n_H is the hydrogen number density of the gas exposed to an X-ray flux F) and photon index of the illuminating power law (which has been taken to be one and the same with the direct power law). The key blurring parameters are those already introduced above for the LAOR shape, i.e. inner radius r_{in} , emissivity index q and disc inclination. The disc outer radius is usually hard to constrain and has been fixed to $400 r_g$. The normalizations of the power-law and reflection components are not tied to each other: in fact, in the presence of light bending effects (e.g. Miniutti & Fabian 2004) which may focus the illuminating radiation on to the disc violating isotropy, the traditional reflection fraction has no clear link with the geometrical covering factor. As a consequence, in this work we simply weight the contribution of the reflection components by measuring the ratio between the reflected and total observed flux.

The blurred reflection model illustrated so far is able to reproduce all the spectral complexity of Ark 120 leaving no clear structure in the residuals (see Fig. 3). However, it is necessary to discuss in more detail the best-fitting parameters that come to light (Table 2). In particular, the disc emissivity profile is suggested to be very steep ($q > 6.2$, consistent with the largest value allowed in the model, which is 10). This would imply that energy dissipation is extremely concentrated in the disc inner regions, virtually all the emission arising within $\sim 2\text{--}3 r_g$. Also, an inclination of 57° seems to be too large for a source with such a clean line of sight, although a misalignment of the accretion disc with the obscuring material is possible (see Lawrence & Elvis 2010).³

³ We note that the host of this Seyfert nucleus is a low-inclination ($i \sim 26^\circ$) spiral galaxy (Nordgren et al. 1995).

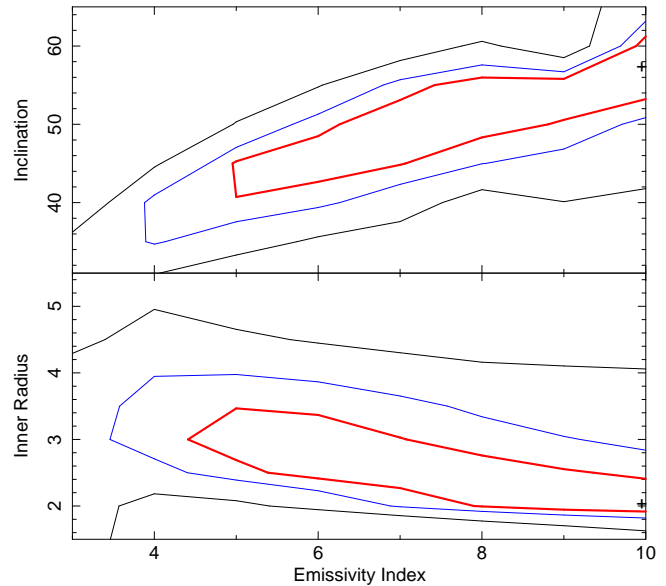


Figure 4. Contour plots (68, 90, 99 per cent confidence levels) showing the degeneracy among the critical blurring parameters. The emissivity index (horizontal axis) appears to be poorly constrained against the disc inclination (vertical axis, upper panel) and inner radius (vertical axis, lower panel). The crosses mark the best-fitting solution when all the three parameters are free to vary.

Indeed, it turns out that at this level of signal-to-noise the critical blurring parameters can be highly degenerate with each other, as shown in Fig. 4. Specifically, the emissivity index appears to be poorly constrained with respect to the inner radius and the disc inclination. We have therefore performed again all the fitting procedure, after freezing in turn each one of these three key parameters to a more convincing value, that is $q = 5$, $r_{in} = 3 r_g$ and $\theta = 40^\circ$ (all obtained from the intermediate analytical steps). In all of these attempts we are able to recover a fit that is statistically equivalent to the one of reference: according to an F -test, the ancillary fits match the general case at a confidence level of 26, 15 and 31 per cent, respectively.⁴ In the light of these considerations, we can conclude that the blurred reflection model provides a valuable interpretation of the broadband X-ray emission of Ark 120 without requiring any extreme parameter.

Owing to the degeneracy discussed above, it is not possible to put solid constraints on the black hole spin, as recently done e.g. in the case of Fairall 9 (Schmoll et al. 2009). In this effort we have switched to a different relativistic kernel (KERRCONV; Brenneman & Reynolds 2006), which allows the dimensionless spin parameter $a = cJ/GM^2$ to vary, assuming that the disc extends down to the innermost stable circular orbit (J and M are the black hole angular momentum and mass). The former q – r_{in} degeneracy is shifted into a q – a degeneracy; yet, by freezing again $q = 5$ we find that $0.24 < a < 0.93$ at a 99 per cent confidence level, with a

⁴ The caveats against the use of the F -test for X-ray spectral analysis (e.g. Protassov et al. 2002) mainly concern the detection of marginal lines. This is not the case here, and the F -test is only intended to assess the degree of degeneracy among the key parameters.

best estimate of $a \simeq 0.74$. It should be noted that the blurring parameters required to model properly the soft excess do not show an obvious agreement with those fitting separately the broad iron line through the same LAOR profile, as pointed out in the previous section. In the framework of a pure disc reflection model, a substantial discrepancy in the blurring/ionization parameters of the soft excess and the companion broad iron K line is not expected. Anyway, we remark that the critical quantities listed in Table 2 should not be taken at their face value, due to the large degeneracy. Indeed, even after freezing $r_{\text{in}} = 10 r_g$ we still obtain a fully acceptable fit⁵ with $\chi^2_\nu \simeq 0.89$. In addition, it has already been suggested that the line detection can be difficult with present data quality unless some favourable conditions are met, e.g. a high iron abundance and/or a reflection-dominated spectrum (as for 1H0707–495; Zoghbi et al. 2010). By inspecting carefully the residuals in the ~ 5 – 7.5 keV energy range, tentative evidence of some unfitted structure is found. We have therefore frozen the best-fitting model altogether and tried to add a gaussian profile, realizing that the residuals are significantly smoothed after the marginal detection of a narrow line centred at $6.69(\pm 0.06)$ keV, whose EW is < 29 eV. If included in the model from the beginning, this line cannot be distinguished with such precision.⁶ Using Fig. 2 as a reference, it seems plausible that the iron K-shell feature in Ark 120 consists of three narrow components (due to neutral, He-like and H-like iron) plus a faint relativistic disc line, whose parameters cannot actually be constrained against the blurring of the soft excess.

It is significant that the narrow lines are not accounted for by the self-consistent reflection model we have adopted. This notwithstanding, an origin different than fluorescence in material exposed to intense X-ray illumination is difficult to consider. We stress that only the putative H-like line keeps unchanged the properties (i.e. a central energy of ~ 6.97 keV and an EW of ~ 30 eV) already found in the analysis restricted to the iron region. Conversely, the line at lower energy is no longer fully consistent with neutral iron emission (it peaks at ~ 6.46 keV), and its EW is significantly reduced (~ 38 eV). This is because genuine neutral iron emission is now embodied in the cold reflection component (see Fig. 3). These two lines then point to intermediate/high ionization states of iron, and may arise in a much more internal environment. In order to probe this possible location, we have again left the width of these lines free, achieving a marginal improvement ($\Delta\chi^2 \simeq -3.7$ with the loss of one degree of freedom, so that the probability of chance improvement is non-negligible). All the previous best-fitting parameters are remarkably confirmed, and the resulting width of $\sigma \simeq 80(\pm 50)$ eV corresponds to a FWHM velocity of $8.7(\pm 4.3) \times 10^3$ km s⁻¹, which is consistent with an origin in (or slightly internal to) the optical BLR. The emission lines seem therefore to be connected to reflection neither at the pc nor at the r_g scale. A possible explanation hints at some blobs of material orbiting in the outskirts

of the disc, forming a sort of X-ray BLR as suggested by Blustin & Fabian (2009), or where the height-radius relation of the disc changes.

Finally, we briefly comment on the relative amplitudes of the reflection components, which have been computed in terms of fractional contributions to the observed flux in both the XIS and the HXD energy range. Shortward of ~ 10 keV, the cold reflector accounts for ~ 4 per cent of the received emission, its significance growing at higher energies where the Compton hump comprises ~ 18 per cent of the total flux (or equivalently ~ 30 per cent with respect to the power-law component only). This strength can be compared to that expected from a slab subtending a solid angle of 2π at the illuminating source by performing a straightforward test with a simple POWERLAW+PEXRAV model (Magdziarz & Zdziarski 1995) in XSPEC. Recalling that PEXRAV includes only the reflected continuum, hence a sound comparison with REFLIONX is possible only beyond ≈ 2 keV, we find a remarkable agreement between our measure and the ‘dummy’ estimate. It is worth noting that even in the presence of strong light bending effects in the inner regions of the disc, at large distance from the X-ray source isotropy should be recovered: it is therefore desirable for the cold reflector identifiable with the obscuring torus to see the same illuminating radiation as the observer at infinity. Such a prescription is entirely complied with in this case. The fractional contribution of the warm reflection component from the disc is instead rather flat, increasing with energy from ~ 19 at 0.5 – 12 keV to only ~ 22 per cent at 12 – 40 keV. Again, these values do not pose severe problems in terms of the required reflection efficiency below ~ 10 keV, due to the wealth of soft X-ray emission lines that are not implemented in the standard PEXRAV/PEXTRIV models; besides this, it is reasonable to allow for moderate light bending involving the blurred component.

In conclusion, a model consisting of both a warm reflection component arising from the photoionized disc surface, blurred by relativistic effects, and a cold one ascribable to a much more distant reprocessor proves to be successful in reproducing the broadband X-ray spectrum of Ark 120. Limited to this peculiar source, this scenario stands as the most convincing among those presented so far, also due to the minimal set of geometrical and physical assumptions involved.

3.3 Alternative models

As we have already mentioned in the introduction, several other models have been adopted in the last decade to fully reproduce the high-quality ~ 0.5 – 10 keV spectra of AGN provided by *Chandra* and/or *XMM-Newton*, specifically concerning the soft excess component. Over the years, most of these interpretations have been either discarded as too phenomenological or disputed because of some physical limitations. Nevertheless, for the sake of a fitting comparison extending up to ~ 40 keV against the blurred reflection model, we have also explored some of the most common alternatives, on which we give a brief report in this section. All the models listed below differ from that based on blurred reflection only in the ingredients apt to describe the soft excess. In particular, they all require a cold reflection component with iron abundance ~ 1.1 – 1.5 (± 0.4), accounting for ~ 4 – 6 and ~ 20 – 30 per cent of the XIS and HXD/PIN observed

⁵ Interestingly, in this case the disc inclination is $\sim 25^\circ$, in excellent agreement with that of the host galaxy. The emissivity index is steep (~ 7.9) but again is poorly constrained.

⁶ Moreover, even if a third narrow line is added to the best fit of the iron feature alone obtained before, the fit does not improve with any statistical significance.

Table 2. Best-fitting parameters for the blurred reflection model of the whole 0.5–40 keV *Suzaku* spectrum.

Γ^a	$2.030^{+0.011}_{-0.004}$	ξ_b^d	278^{+35}_{-27}
E_1	$6.46^{+0.02}_{-0.03}$	q	> 6.2
E_2	6.97 ± 0.04	r_{in}	$2.04^{+1.58}_{-0.27}$
σ	10^*	θ	57^{+5}_{-12}
EW_1	38^{+32}_{-28}	R_d^e	$0.034^{+0.003}_{-0.004}$
EW_2	32^{+11}_{-12}	R_b^e	$0.178^{+0.030}_{-0.015}$
Fe^b	$0.73^{+0.14}_{-0.06}$	F_{obs}^f	$5.29^{+0.28}_{-0.08}$
ξ_d^c	< 10.4	χ^2_ν	$410.4/468$
<hr/>			
Fe	$0.77^{+0.09}_{-0.10}$	r_{in}	$3.03^{+0.76}_{-0.65}$
ξ_b	280^{+47}_{-29}	θ	42^{+5}_{-4}
q	5.0^*	χ^2_ν	$411.5/469$
<hr/>			
Fe	0.77 ± 0.13	r_{in}	3.00^*
ξ_b	278^{+45}_{-29}	θ	44^{+3}_{-6}
q	$5.7^{+2.6}_{-1.9}$	χ^2_ν	$411.3/469$
<hr/>			
Fe	$0.77^{+0.13}_{-0.09}$	r_{in}	$3.30^{+0.33}_{-0.61}$
ξ_b	279^{+46}_{-28}	θ	40^*
q	$4.8^{+1.5}_{-1.0}$	χ^2_ν	$412.3/469$

^a Photon index.^b Iron abundance, in solar units.^c Ionization parameter of the distant reflector, in erg cm s^{-1} .^d Ionization parameter of the blurred reflector, in erg cm s^{-1} .^e Reflection fraction over the 0.5–10 keV range.^f Observed 0.5–10 keV flux, in $10^{-11} \text{ erg cm}^{-2} \text{ s}^{-1}$.

flux, respectively, and also for the narrow emission feature at 6.4 keV. Other two unresolved gaussian lines are always needed in the 6.47–6.70 and 6.93–7.01 keV range: even if loosely consistent with He-like iron emission, the former is apparently trying to compensate somehow for the lack of the broadened disc line. In the following, we just provide the key parameters of the soft excess component in some illustrative cases.

1) *Blackbody* ($\chi^2_\nu/\text{d.o.f.} = 0.995/471$): the best-fitting disc temperature is ~ 0.14 keV, and therefore lies in the range characteristic to the thermal scenario. No significant improvement can be obtained by adopting a more realistic (e.g. multicolour) blackbody profile.

2) *Broken power law* ($\chi^2_\nu/\text{d.o.f.} = 0.963/471$): as one can immediately see from Fig. 1, a double-sloped power law is sufficient to achieve a good fit to the low-energy spectrum. The soft photon index is ~ 2.33 , the hard one is ~ 2.00 ; the break-point energy is established at 1.73 keV.

3) *Smeared absorption* ($\chi^2_\nu/\text{d.o.f.} = 1.02/470$): we have used the SWIND1 model to mimic absorption in a partially ionized relativistic gas, even if the latest simulations of the velocity and density structure of any possible accretion disc wind or outflow rule out this scenario as the origin of a smooth soft excess (Schurch et al. 2009). The column density of the putative absorber is $N_{\text{H}} \simeq 17 \times 10^{22} \text{ cm}^{-2}$, and the ionization parameter is $\log \xi \simeq 3.3$. The gaussian velocity dispersion in this warm gas is the maximum allowed, i.e. $v/c = 0.5$. Since the power-law index is slightly steeper than usual, being ~ 2.12 , this model presents larger deviations from the data at the higher energies.

4) *Cold Comptonization* ($\chi^2_\nu/\text{d.o.f.} = 0.918/470$): many codes with a different degree of complexity are available to describe Comptonization (e.g. Poutanen and Svensson

1996). However, it is not possible to put firm constraints on the plasma properties and geometrical structure with the present data quality and energy coverage; we have therefore adopted the essential COMPTT code of Titarchuk (1994). The exact temperature of seed photons is not very important, provided that its value is reasonably low, so it has been frozen to 50 eV as broadly presumable for a source like Ark 120. The cold corona turns out to have an electron temperature of ~ 0.28 keV with an optical depth of ~ 13 , even if the two parameters are expected to be degenerate to some extent. This optically thick soft component has a luminosity of $\sim 10^{43} \text{ erg s}^{-1}$, and can be roughly approximated by a blackbody. This gives a size of the emitting region of $\sim 4 \times 10^{11} \text{ cm}$, whereas $r_{\text{g}} \sim 2 \times 10^{13} \text{ cm}$ (the mass of the black hole in Ark 120 is estimated from reverberation mapping to be $M_{\text{BH}} \simeq 1.5 \times 10^8 M_{\odot}$; Peterson et al. 2004). Summarizing, the Comptonization scenario can be regarded at present as the only physical alternative to the blurred reflection model in order to account for the soft excess of Ark 120, but its details are difficult to probe; the argued compactness of the soft X-ray emitting region represents a further problem for the nature and the geometry of the Comptonizing plasma.

3.4 Timing analysis

In addition to spectral fitting, the other fundamental approach to understand the properties of the central engine in AGN is the study of variability. In principle, the latter can also provide independent information to discriminate between the cold Comptonization and the blurred reflection scenario for the soft excess, since the two models make quite divergent predictions about the behaviour of the source in

the time domain. In a very simplistic way, the time lags affecting the different energy bands that have been observed in many AGN can be regarded as a natural consequence of a Comptonization process: the time delay between the hard and the soft X-ray variations is due to the larger number of scattering events that the high-energy photons have to experience before escaping to infinity. However, matters appear to be much more complicated than this naive picture (e.g. Arévalo & Uttley 2006; McHardy et al. 2007). On the other hand, if the soft excess is a reflection signature, the soft band should lag behind the hard power-law component as expected in a reverberation context, after singling out the timescale corresponding to the light crossing time from the primary source to the reflector and back. Evidence in this sense has been recently found in 1H0707–495 (Fabian et al. 2009; Zoghbi et al. 2010).

Although *Suzaku* is not an ideal observatory to carry out detailed timing studies of AGN, mainly because of the frequent gaps induced by the short orbital period, it is worth checking the variability pattern of Ark 120 for possible hints. The total XIS light curve is shown in Fig. 5, and displays a very gentle variation, in part expected due to the large black hole mass. Using a time resolution of 500 s, the fractional *rms* variability amplitude F_{var} (defined as in Vaughan et al. 2003) is $9.1(\pm 0.2)$ per cent over the 0.5–10 keV range.⁷ In order to check for a possible energy dependence, we have computed the individual variability amplitudes in four energy bands (0.5–1, 1–2, 2–5 and 5–10 keV), which turn out to be $8.7(\pm 0.4)$, $9.7(\pm 0.2)$, $9.1(\pm 0.3)$ and $8.5(\pm 0.7)$ per cent, respectively. This does not provide any straightforward indication for different variability patterns, and these are likely to be actually consistent with each other. Moreover, we note that the four bands above cannot be clearly linked to different spectral components, since the direct power law is dominant over the whole spectrum of Ark 120. Incidentally, the shape of the HXD/PIN light curve closely resembles the trend observed in the XIS range, although in this case $F_{\text{var}} = 19.1(\pm 3.4)$, due to the larger noise. A similar indication in favour of a coarse coherence with no lags among the energy bands comes from the 1–2, 2–5 and 5–10 over 0.5–1 keV hardness ratios (Fig. 5), which are all well-fitted with a constant value ($\chi^2/\text{d.o.f} \simeq 246/231$, $252/231$ and $267/231$, corresponding to null hypothesis probabilities of 24, 16 and 5 per cent, respectively). The lack of differential variability was also found by De Marco et al. (2009), who have analyzed the *XMM-Newton* spectrum focusing on the iron K line region. The total time elapsed in this *Suzaku* observation is ~ 185 ks, corresponding to ~ 1.2 keplerian orbital periods at $10 r_g$ (e.g. Bardeen, Press & Teukolsky 1972). It is therefore unlikely to reveal dramatic changes on such timescales, despite the small radii involved.

In short, the timing analysis of Ark 120 is inconclusive and does not point to any specific physical model. Yet, by confirming that the source variations involve the flux amplitude only, it offers substantial support to our previous spectral

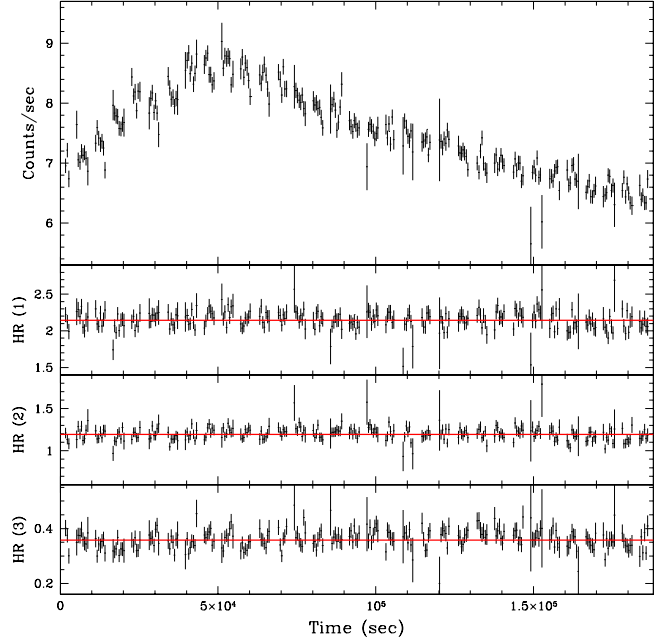


Figure 5. Top panel: 0.5–10 keV background-subtracted light curve of Ark 120, summed over the three XIS detectors and plotted adopting a time resolution of 500 s. The flux variation is rather gentle, with an overall *rms* variability amplitude of ~ 9 per cent. Lower panels: respectively from above, 1–2, 2–5 and 5–10 over 0.5–1 keV hardness ratios, which turn out to be remarkably stable over the entire observation; the red solid lines show the best-fitting constant values. (Note: the outlying points with large error bars correspond to the ends of a single *Suzaku* orbit, and are just artifacts of the time binning).

study, given that the average X-ray emission genuinely represents the single physical state in which the source was caught during the *Suzaku* observation.

3.5 The 2003 *XMM-Newton* observation

Previously to *Suzaku*, Ark 120 was monitored by *XMM-Newton* on 2003 August 24–25. A detailed study of this observation is presented in Vaughan et al. (2004). In particular, a wide range of models (including reflection components, disc blackbodies, bremsstrahlung and thermal Comptonization) were tested in order to give an adequate description of the broadband spectrum; yet, none of these was able to account for the properties of the soft excess. It is not our aim to perform the same comprehensive analysis over again, reproducing equivalent results. Since then, anyway, the available reflection models have been substantially upgraded, after Ross & Fabian (2005). So it is worth reviewing the very high-quality *XMM-Newton* observation in the light of the blurred reflection scenario we have developed in this work. Our reduction follows that illustrated in Vaughan et al. (2004), and yields to a full agreement of the final data products. The following analysis concerns the EPIC-pn spectrum only, and is confined to the 0.5–10 keV energy range for consistency with the *Suzaku* XIS operational window. Moreover, due to the large count rate in the soft band the ionization and blurring parameters are highly sensitive to calibration uncertainties, which can be quite large below ~ 0.6 keV (see also Papadakis

⁷ All the values reported in this section have little dependence on the adopted time bin. This does not undermine the general conclusions: in this source, the light crossing time over a distance of $1 r_g$ is ~ 750 s, so that most of the variability is expected to take place on larger timescales.

Table 3. Best-fitting reflection parameters for the 2003 *XMM-Newton* observation.

Γ	$2.116^{+0.011}_{-0.009}$	$\xi_{b,1}$	299^{+20}_{-18}
E_1	$6.40^{+0.02}_{-0.01}$	$\xi_{b,2}$	< 13.9
E_2	$6.64^{+0.03}_{-0.04}$	q	$5.2^{+0.4}_{-0.3}$
E_3	7.00 ± 0.03	r_{in}	$2.26^{+0.11}_{-0.07}$
σ	10^*	θ	50^*
EW_1	47^{+23}_{-22}	R_d	< 0.008
EW_2	26 ± 7	$R_{b,1}$	$0.218^{+0.013}_{-0.016}$
EW_3	25 ± 15	$R_{b,2}$	$0.062^{+0.010}_{-0.008}$
Fe	0.75^*	F_{obs}	$6.80^{+0.44}_{-0.18}$
ξ_d	1.0^*	χ^2_ν	$2044/1857$

et al. 2010).

The spectral shape and flux level in the two observations are remarkably similar, hence we have directly applied the best-fitting model obtained for the *Suzaku* case. Iron abundance and disc inclination are obviously not time-dependent parameters, and have been frozen to 0.75 (solar units) and 50° , respectively. Under these assumptions we obtain a reasonable fit to the data, even if not formally acceptable in a statistical sense ($\chi^2_\nu \sim 1.16$), as quite usual at the highest levels of data quality. A further improvement can be achieved by allowing for a slightly larger degree of complexity in the model. First, a third narrow line is included for He-like iron emission as also pointed out by Brenneman & Reynolds (2009). Second, we introduce an additional reflection component, subject to the same relativistic smearing but with an independent ionization parameter, in order to allow for possible non-uniformity within the disc. As a result, this extra component turns out to require a low ionization, while the cold distant reflection becomes negligible. The value of $\chi^2_\nu/\text{d.o.f.}$ drops to $\sim 1.10/1857$ and the best-fitting key parameters are very well-matched to those obtained for the *Suzaku* observation (see Table 3). Conversely, beyond the iron feature there remains some excess emission that cannot be fitted by increasing the model complexity. These deviations of the model from the data are of the order of ~ 10 per cent at most (Fig. 6). We note that if the disc inclination is left free to vary, a value around $\sim 80^\circ$ (see also Nandra et al. 2007) is able to offset any ~ 8 – 10 keV excess, while the iron abundance is not a critical parameter in this sense. Interestingly, the Galactic column density converges towards the upper limit of the admitted range: if instead N_H is frozen to the lower value the fit quality marginally worsens, but the free parameters smoothly resetttle so that the picture above is not modified. We have also checked the behaviour of the model down to 0.3 keV: a very clean bump in the data/model ratio emerges at 0.3–0.5 keV. After freezing the best-fitting model, this feature is quite well-reproduced by a blackbody of temperature ~ 40 eV, even if the residuals in the 0.3–0.7 keV range display some tentative structure. Finally, we have tested for completeness the cold Comptonization model: in this case, the parameters of the soft corona are in excellent agreement with those found above for the *Suzaku* spectrum, but the fit is less accurate ($\chi^2_\nu \sim 1.19$) and large residuals remain in the 0.5–0.7 and 5.5–7 keV range. Our revision of the high-quality *XMM-Newton* observation seems therefore to confirm the reliability of the

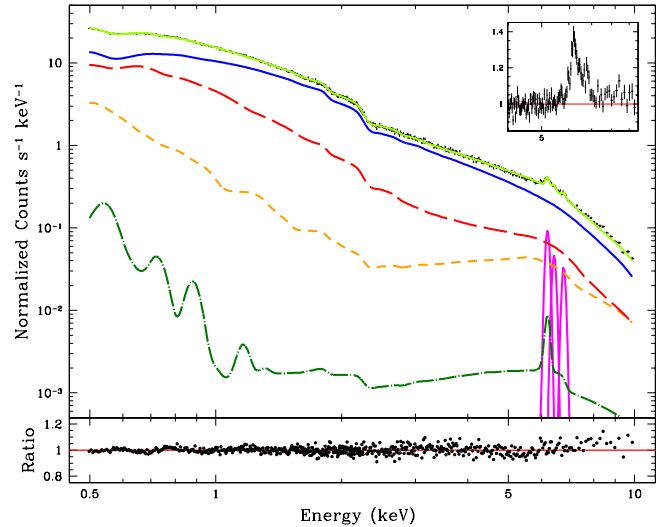


Figure 6. Top panel: as Fig. 3 but for the 2003 *XMM-Newton* observation, with the same code. The additional cold/blurred reflection component is plotted in orange (short-dashed line). The inner box shows the profile of the iron feature, obtained as the ratio over a simple power-law trend. Bottom panel: data/model ratio to the best fit, emphasizing the slight excess emission longward of the iron feature. Errors bars are omitted for clarity.

blurred reflection interpretation for soft X-ray emission of Ark 120.

4 CONCLUSIONS

We have reported on a long *Suzaku* observation of Ark 120, one of the few known examples of nearly absorption-free active nuclei. This ‘bare’ BLS1 galaxy is the optimal candidate to investigate the nature of the ubiquitous soft excess observed in the X-ray spectra of unobscured AGN. Its broadband 0.5–40 keV spectrum reveals a significant curvature with respect to the main power-law component, as excess emission is found at both low (< 2 keV) and high (> 10 keV) energies. Also, a complex iron K-shell feature is clearly detected at ~ 5 – 7 keV, showing a structured profile in which can be identified two (three, tentatively) narrow gaussian cores originating roughly at the BLR scale, and a relativistically skewed line arising from the disc at $r \gtrsim 10 r_g$. The latter, even if not as prominent as in the most impressive cases, cannot be interpreted through a blend of unresolved

lines or a system of multiple absorbers. Hence relativistic effects have to be included in the broadband analysis.

We have shown that all the spectral complexity can be successfully explained in terms of a self-consistent reflection model, allowing for both a warm/blurred and a cold/distant reflection component. In this picture, the reprocessing of the primary X-ray radiation takes place in two distinct regions, that can be plainly identified with the inner accretion disc ($r \lesssim 10 r_g$) and the far-off obscuring torus. Depending on the exact geometry, however, additional physical locations (e.g. a belt of orbiting clouds) may contribute, since fluorescent iron emission suggests the existence of a wide range of ionization states. This blurred reflection scenario is further corroborated after reviewing a previous high-quality *XMM-Newton* observation of Ark 120. Therefore, as for this single source, the present interpretation stands as the most convincing among those that have been proposed so far, due to the minimal set of geometrical and physical assumptions involved.

In general it is difficult to rely on comparably clean lines of sight to the nuclear regions, and we expect that other processes (likely non-thermal Comptonization, warm absorption, reprocessing in winds/outflows) also play a non-negligible role in shaping the X-ray emission of type 1 AGN. As a consequence, our aim in the near future is to extend this study to a large sample of low-obscuration sources, possibly observed by both *Suzaku* and *XMM-Newton* to combine the high-energy coverage of the former and the large effective area of the latter. This will allow us to infer the average contribution of blurred disc reflection to the soft excess and to the X-ray luminosity of AGN, and at the same time to test the basic predictions of the light bending model and to explore the nature of the illuminating source itself. We note that if blurred reflection is really the dominant component of the soft excess, the black hole spin distribution may be biased towards the larger values; indeed, it has already been suggested in many previous works (e.g. Volonteri et al. 2005) that the supermassive black holes in AGN should be rapidly rotating. Even if the spin cannot be firmly constrained in Ark 120 due to the large degeneracy among the blurring parameters (but provisionally $a \simeq 0.7$), our case study is apparently consistent with this scenario.

ACKNOWLEDGMENTS

EN acknowledges financial support from the ASI-INAF I/088/06/0 contract. ACF thanks the Royal Society. RCR and DJW acknowledge the financial support provided by STFC. The authors are also grateful to the anonymous referee for the constructive comments.

REFERENCES

Arévalo P., Uttley P., 2006, MNRAS, 367, 801
 Arnaud K. A., et al., 1985, MNRAS, 217, 105
 Blustin A. J., Fabian A. C., 2009, MNRAS, 399, L169
 Blustin A. J., Page M. J., Fuerst S. V., Branduardi-Raymont G., Ashton C. E., 2005, A&A, 431, 111
 Boller T., Brandt W. N., Fink H., 1996, A&A, 305, 53
 Brandt W. N., Fabian A. C., Nandra K., Tsuruta S., 1993, MNRAS, 265, 996

Brenneman L. W., Reynolds C. S., 2006, ApJ, 652, 1028
 Brenneman L. W., Reynolds C. S., 2009, ApJ, 702, 1367
 Coppi P. S., 1999, in Poutanen J., Svensson R., eds, ASP Conf. Ser. Vol. 161, High Energy Processes in Accreting Black Holes. Astron. Soc. Pac., San Francisco, p. 375
 Crenshaw D. M., Kraemer S. B., Boggess A., Maran S. P., Mushotzky R. F., Wu C.-C., 1999, ApJ, 516, 750
 Crenshaw D. M., Kraemer S. B., George I. M., 2003, ARA&A, 41, 117
 Crummy J., Fabian A. C., Gallo L., Ross R. R., 2006, MNRAS, 365, 1067
 De Marco B., Iwasawa K., Cappi M., Dadina M., Tombesi F., Ponti G., Celotti A., Miniutti G., 2009, A&A, 507, 159
 Dewangan G. C., Griffiths R. E., Dasgupta S., Rao A. R., 2007, ApJ, 671, 1284
 Dickey J. M., Lockman F. J., 1990, ARA&A, 28, 215
 Fabian A. C., Ballantyne D. R., Merloni A., Vaughan S., Iwasawa K., Boller T., 2002, MNRAS, 331, L35
 Fabian A. C., et al., 2009, Natur, 459, 540
 Gallo L. C., Boller T., Tanaka Y., Fabian A. C., Brandt W. N., Welsh W. F., Anabuki N., Haba Y., 2004, MNRAS, 347, 269
 George I. M., Fabian A. C., 1991, MNRAS, 249, 352
 Gierliński M., Done C., 2004, MNRAS, 349, L7
 Grupe D., 2004, AJ, 127, 1799
 Haardt F., Maraschi L., 1991, ApJ, 380, L51
 Haardt F., Maraschi L., 1993, ApJ, 413, 507
 Kalberla P. M. W., Burton W. B., Hartmann D., Arnal E. M., Bajaja E., Morras R., Pöppel W. G. L., 2005, A&A, 440, 775
 Koyama K., et al., 2007, PASJ, 59, 23
 Laor A., 1991, ApJ, 376, 90
 Lawrence A., Elvis M., 2010, ApJ, 714, 561
 Magdziarz P., Zdziarski A. A., 1995, MNRAS, 273, 837
 McHardy I. M., Arévalo P., Uttley P., Papadakis I. E., Summons D. P., Brinkmann W., Page M. J., 2007, MNRAS, 382, 985
 Miniutti G., Fabian A. C., 2004, MNRAS, 349, 1435
 Miniutti G., et al., 2007, PASJ, 59, 315
 Miniutti G., Ponti G., Greene J. E., Ho L. C., Fabian A. C., Iwasawa K., 2009, MNRAS, 394, 443
 Mitsuda K., et al., 2007, PASJ, 59, 1
 Nandra K., O'Neill P. M., George I. M., Reeves J. N., 2007, MNRAS, 382, 194
 Nordgren T. E., Helou G., Chengalur J. N., Terzian Y., Khachikian E., 1995, ApJS, 99, 461
 Page K. L., Turner M. J. L., Done C., O'Brien P. T., Reeves J. N., Sembay S., Stuhlinger M., 2004, MNRAS, 349, 57
 Papadakis I. E., Brinkmann W., Gliozzi M., Raeth C., Nicastro F., Conciatore M. L., 2010, A&A, 510, A65
 Peterson B. M., et al., 2004, ApJ, 613, 682
 Ponti G., Miniutti G., Cappi M., Maraschi L., Fabian A. C., Iwasawa K., 2006, MNRAS, 368, 903
 Poutanen J., Svensson R., 1996, ApJ, 470, 249
 Bardeen J. M., Press W. H., Teukolsky S. A., 1972, ApJ, 178, 347
 Protassov R., van Dyk D. A., Connors A., Kashyap V. L., Siemiginowska A., 2002, ApJ, 571, 545
 Remillard R. A., McClintock J. E., 2006, ARA&A, 44, 49
 Ross R. R., Fabian A. C., 1993, MNRAS, 261, 74
 Ross R. R., Fabian A. C., 2005, MNRAS, 358, 211
 Sani E., Lutz D., Risaliti G., Netzer H., Gallo L. C., Trakhtenbrot B., Sturm E., Boller T., 2010, MNRAS, 403, 1246
 Schmoll S., et al., 2009, ApJ, 703, 2171
 Schurch N. J., Done C., 2007, MNRAS, 381, 1413
 Schurch N. J., Done C., Proga D., 2009, ApJ, 694, 1
 Shemmer O., Netzer H., 2002, ApJ, 567, L19
 Sobolewska M. A., Done C., 2007, MNRAS, 374, 150
 Takahashi T., et al., 2007, PASJ, 59, 35
 Titarchuk L., 1994, ApJ, 434, 570
 Turner T. J., Pounds K. A., 1989, MNRAS, 240, 833

- Vaughan S., Edelson R., Warwick R. S., Uttley P., 2003, MNRAS, 345, 1271
- Vaughan S., Fabian A. C., Ballantyne D. R., De Rosa A., Piro L., Matt G., 2004, MNRAS, 351, 193
- Volonteri M., Madau P., Quataert E., Rees M. J., 2005, ApJ, 620, 69
- Wandel A., Peterson B. M., Malkan M. A., 1999, ApJ, 526, 579
- Ward M., Elvis M., Fabbiano G., Carleton N. P., Willner S. P., Lawrence A., 1987, ApJ, 315, 74
- Wilms J., Allen A., McCray R., 2000, ApJ, 542, 914
- Zoghbi A., Fabian A. C., Uttley P., Miniutti G., Gallo L. C., Reynolds C. S., Miller J. M., Ponti G., 2010, MNRAS, 401, 2419